Phase transition of RbH$_2$PO$_4$ and its composite with SiO$_2$ studied by thermal analysis

Zikun Li · Wingkin Edward Chan

Abstract The phase transition at T_p (~ 109 °C) of RbH$_2$PO$_4$ and its composite with SiO$_2$ has been investigated by thermal analysis here. In the case of neat RbH$_2$PO$_4$, there is a linear relationship between endothermic peak temperature (T_m) and square root of heating rate ($\Phi^{1/2}$), from which the onset temperature of phase transition can be determined. Besides, Kissinger method and another calculation method were employed to obtain the activation energy of phase transition. The detailed deduction process was presented in this paper, and the estimated activation energies are $E_1 \approx 126.3$ kJ/mol and $E_2 \approx 129.2$ kJ/mol, respectively. On the other hand, the heterogeneous doping of RbH$_2$PO$_4$ with SiO$_2$ as dopant facilitates its proton conduction and leads to the disappearance of jump in conductivity at T_p. The heats of transition in the composites decrease gradually with increasing the molar fraction of SiO$_2$ additives. In the cooling process, a new and broad exothermic peak appeared between ~ 95 and ~ 110 °C, and its intensity also changes with the SiO$_2$ amount. These phenomena might be related to the formation of amorphous phase of RbH$_2$PO$_4$ on the surface of SiO$_2$ particles due to the strong interface interaction.

Keywords RbH$_2$PO$_4$ · Composite · Phase transition · Activation energy · Heat of transition

Introduction

Fuel cells operative at intermediate-temperature (IT) are attractive power generation systems from the aspect of energy conversion efficiency. Recently, solid acid fuel cells employing CsHSO$_4$ and CsH$_2$PO$_4$ as electrolytes have been successfully demonstrated [1, 2], much more attention was paid to these materials because of their thermal stability, anhydrous proton conduction, and environmentally friendly nature. As one member of solid acid family, RbH$_2$PO$_4$ has been investigated for almost two decades and its ambient and sub-ambient phases have been well characterized: it has an orthorhombic structure with space group $Fdd2$ below its ferro-paraelectric phase transition at $T_c = -126$ °C, and a tetragonal structure with space group $I\overline{4}2d$ at room temperature [3]. However, its high-temperature (HT) phases are less certain. From X-ray diffraction (XRD) experiments Blinc et al. [4] found that it transforms from tetragonal to monoclinic symmetry at $T_p = 86$ °C. Further studies have followed, based primarily on thermal analysis, proton magnetic resonance, XRD and so on [5, 6], and the monoclinic phase of RbH$_2$PO$_4$ has been confirmed to belong to the space group $P2_1/a$ [6]. However, the measured transition temperature, T_p, varied by wide margin between ~ 80 and ~ 120 °C strongly depending on the experimental conditions [3]. Later, it was suggested that absorbed water on the surface of sample acts as a catalyst that triggers the tetragonal–monoclinic phase transition, because pretreatment with water showed that the enthalpy at T_p depends on the water partial pressure and the duration of contact with water vapor. On the other hand, RbH$_2$PO$_4$ exhibited an abrupt jump in the proton conductivity upon heating above this temperature threshold T_p [7]. This important property is so-called "superprotonic" behavior, and such high proton conductivity is just the "high point" attracting the most attention due to its potential application in fuel cell electrolyte membrane. To further uncover the microscopic mechanisms responsible for the enhanced proton conductivity, a great deal of investigation has been done very

Z. Li (✉) · W. E. Chan
Department of Physics, Hong Kong Baptist University,
224 Waterloo Road, Kowloon, Hong Kong, China
e-mail: 08466173@hkbu.edu.hk

recently. Some research groups attributed this proton conductivity enhancement to structural transition from tetragonal to monoclinic phase at T_p [7, 8]. However, others have claimed that the heating induced dehydration and chemical decomposition/polymerization via the reaction:

$$4RbH_2PO_4 \rightarrow 2RbH_2PO_4 \cdot Rb_2H_2P_2O_7 + H_2O \qquad (1)$$

lead to the HT behavior [9–12]. Besides, they proposed a model where the proton conductivity enhancement is attributable to the rapid breaking and reforming of H bonds triggered by the above-mentioned chemical decomposition/polymerization [13]. Despite numerous studies, this phenomenon is not well understood and remains a matter of debate. Further investigation of the real nature of RbH_2PO_4 transformation around T_p and ion dynamics in this material are worth carrying out because understanding them is an important step toward optimizing the application of RbH_2PO_4 in fuel cell devices. In the first part of this study, we confirmed the phase transition phenomenon in RbH_2PO_4 through thermal analysis, HT XRD, and measurements of conductivity. In addition, we presented a detailed calculation process of activation energy of phase transition, aiming at better clarifying the structural transformation at T_p.

On the other hand, it is well known that heterogeneous doping of ionic salts with non-conducting oxide particles offers the possibility of producing, in a wide temperature range, high-conductivity composites with enhanced thermal stability and improved mechanical performance [14–16]. Considering the feasibility and practicability of RbH_2PO_4 as fuel cell electrolyte, its HT conductivity enhancement was also worth studying by using this method. In previous work [17], we have indeed observed the enhancement of proton conductivity in RbH_2PO_4/SiO_2 composite in which a strong surface interaction between the components takes place. This interaction leads not only to the stabilization of a new phase on the surface of oxide but also to a change of electrical properties of RbH_2PO_4 bulk at HT. In the second part of present study, our main concern is thus investigation of the influence of SiO_2 particles on the structural transformation of RbH_2PO_4 bulk and its thermal properties at above-mentioned T_p. The results will provide new insight into fundamental aspects of phase transition and the proton conductivity enhancement in the heterogeneous composites.

Experimental

Sample preparation

The RbH_2PO_4 compound under study was prepared from aqueous solutions by mixing stoichiometric amounts of rubidium carbonate (Rb_2CO_3) and phosphorous acid (H_3PO_4) in which the Rb:PO_4 M ratio was fixed at 1:1 according to $Rb_2CO_3 + 2H_3PO_4 \rightarrow 2RbH_2PO_4 + CO_2 + H_2O$. Rapid precipitation of product was then induced by the introduction of methanol, and then the precipitate was filtered out. The final powder was dried and kept in an oven at 80 °C for at least 6 h, both after preparation and prior to all measurements, in view of their hygroscopicity. In the case of RbH_2PO_4-based composites, amorphous SiO_2 particles with specific surface area at $S_{sp} \approx 150$ m^2/g determined by the BET method were used as dispersing matrices of the composites. $(1 - x)RbH_2PO_4$–$xSiO_2$ composites were prepared by using a high-energy ball mill, mechanically milled for 24 h, and the molar fraction of SiO_2 additives was varied from 0 to 0.6, corresponding to 0–50 vol% SiO_2. Then, polycrystalline RbH_2PO_4 or its composite was pressed at 7 tons for 5 min to form pellets (diameter: 10 mm; thickness: ~4 mm). Silver electrodes were attached to both sides of the pellets by silver paint following to silver vapor deposition for impedance measurement.

Characterization and measurements

Powder X-ray diffraction (XRD) patterns of the product were recorded in a Rigaku Rotaflex RU-200B diffractometer using CuK$_\alpha$ radiation ($\lambda = 1.5418$ Å), to confirm their identity. Differential scanning calorimetry (DSC) was performed with a Perkin-Elmer Diamond DSC. In this thermo-analytical experiment, the sample was sat in an aluminum pan, and heated at different heating rates in a dynamic atmosphere of dried N_2 flowing at 50 mL/min. The impedance of RbH_2PO_4 or its composites was measured by alternating current (AC) impedance spectroscopy using an HP 4284A Precision LCR Meter, a frequency range from 20 Hz to 1 MHz and an applied voltage of 1.0 V in air from 25 to 200 °C. Impedance spectra were analyzed using the commercially available software package, Zview (Scribner Associates Inc.). The conductivity, σ, was calculated from resistance, R, and pellet dimension, i.e., $\sigma = L/(AR)$, where L and A are thickness of the pellet and electrode surface area, respectively.

Results and discussion

Phase transition of neat RbH_2PO_4 at T_p

Typical thermal analysis result via multiple cycles of DSC measurement of RbH_2PO_4 sample at a fixed heating rate is presented in Fig. 1. It shows a pronounced endothermic peak at 123 °C on the heating cycle. In subsequent cooling process, the reverse transition exhibits a slight hysteresis (~3 °C), namely, the exothermic peak shifted slightly to
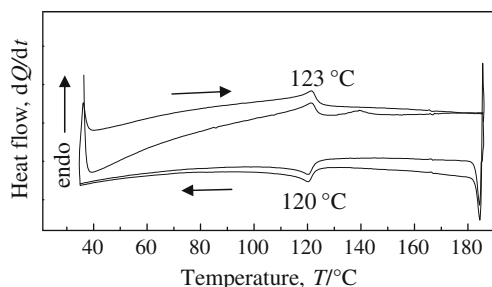
Fig. 1 DSC trace of RbH₂PO₄ for two heating/cooling cycles to 185 °C with a fixed rate of 10 °C/min

120 °C with a heat of transition that is the same in magnitude, within error, of that observed on heating. For the second heating cycle, the transition temperature keeps unchanged, with the heat of transition essentially unchanged and the reverse transition behavior also essentially unchanged. The reproducibility in thermal behavior between a freshly prepared sample and one already exposed to HT indicates that the phenomenon at T_p between ~ 80 and ~ 120 °C is not related to dehydration or thermal decomposition but potential structure transition. On the other hand, the initial dehydration of RbH₂PO₄ takes place at ~ 250 °C, which has been confirmed in our previous report [18]. Moreover, powder XRD data in Fig. 2 were collected at different temperatures under atmospheric condition. The sample was allowed to equilibrate for ~ 30 min at each temperature. Initial measurement at room temperature shows that RbH₂PO₄ has tetragonal phase with space group $I\bar{4}2d$ [3], whose Miller indices assignment to each peak was made according to the ASTM database. No other observable peaks were found. Subsequently, the measurement temperature was raised up to 100 °C at which tetragonal phase was still observed. However, the signal of tetragonal phase disappeared at 125 °C, and a new XRD pattern, i.e., monoclinic phase of RbH₂PO₄ with space group $P2_1/a$ [6] appeared clearly. The difference in XRD patterns at 100 and 125 °C, along with the results of DSC cycles described above, demonstrated that RbH₂PO₄ crystal does undergoes a structural transition from tetragonal to monoclinic phase at T_p.

As a rule, an inherent thermal lag in the thermal analysis can result in systematic errors in true and measured reaction temperatures as a function of heating rate. The difference $(\Delta T = T_m - T_o)$ between the measured peak temperature (T_m) and equilibrium onset temperature (T_o) is proportional to heating rate (Φ), sample mass (m), thermal resistance (R), and transition enthalpy (ΔH), i.e.,

$$\Delta T^2 = 2mR\Phi \cdot \Delta H \tag{2}$$

According to this empirical formula, there should be a linear relationship between ΔT and $\Phi^{1/2}$. As $\Phi \to 0$, $\Delta T = T_m - T_o \to 0$, implying $T_m \to T_o$ [19]. Thus, one
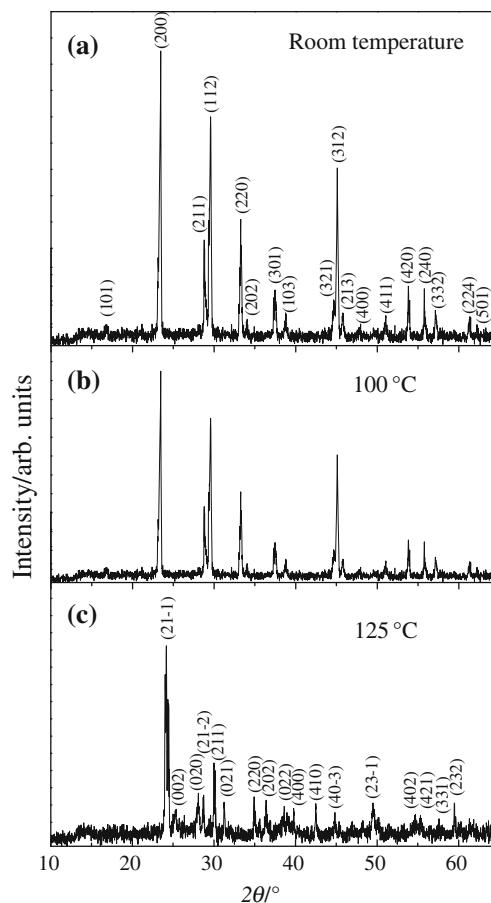

Fig. 2 XRD patterns of as-prepared RbH₂PO₄ at **a** room temperature; **b** 100 °C; **c** 125 °C

can estimate the true onset temperature of phase transition by using this mathematical expression. Therefore, the DSC experiments were carried out at various heating rates of 5, 10, 15, 20, 25 °C/min. As shown in Fig. 3a, the peak temperature (T_m) of DSC signals is strongly dependent on the heating rate (Φ). The smaller the heating rate, the lower the peak temperature of phase transition. In general, this phenomenon is obvious for the first-order phase transition or chemical reaction. The current result is believed to belong to the former case. As an example of the heating-rate dependent thermal behavior of RbH₂PO₄, the T_m values for each heating rate, as measured by DSC, are plotted as a function of $\Phi^{1/2}$ in Fig. 3b. As one can see, a linear relationship between T_m and $\Phi^{1/2}$ is indeed evident. Therefore, the true and equilibrium onset temperature, T_o, could be determined by extrapolating to a heating rate of zero, i.e., $T_o \approx 109$ °C. This value is independent of heating rate and denoted as the phase transition temperature T_p.

In order to derive the activation energy (E) of this phase transition at T_p, the well-known Kissinger–Akahira–Sunose method (KAS method hereafter for short) was used [20].
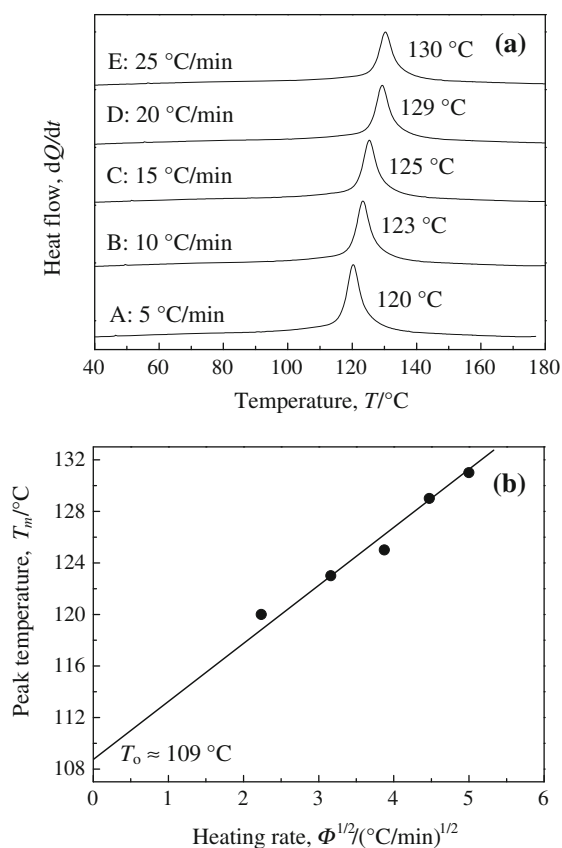
Fig. 3 a Results of DSC thermal analysis carried out at heating rate of 5, 10, 15, 20, and 25 °C/min for neat RbH_2PO_4. **b** Peak temperature of phase transition at T_p as a function of heating rate as measured by DSC

Kissinger suggested that the activation energy can be estimated from the variation of DTA peak temperatures with different heating rates. The kinetics of most solid state reactions can be described by an equation below

$$\frac{dx}{dt} = Af(x)\exp\left(-\frac{E}{RT}\right) = A(1-x)^n\exp\left(-\frac{E}{RT}\right) \quad (3)$$

where x is the reacted fraction ($0 \le x \le 1$), dx/dt the reaction rate, A the preexponential factor of Arrhenius, $f(x) = (1-x)^n$ the reaction kinetic model, n the order of reaction, E the activation energy, T the absolute temperature, R the gas constant ($R = 8.314$ J/mol K). If heating the sample at a constant rate ($\Phi = dT/dt$), then by differentiation of Eq. 3,

$$\frac{d}{dt}\left(\frac{dx}{dt}\right) = \frac{d}{dt}\left[\frac{E\Phi}{RT^2} - An(1-x)^{n-1}\exp\left(-\frac{E}{RT}\right)\right] \quad (4)$$

The maximum rate occurs at a temperature T_m defined by setting Eq. 4 equal to zero, i.e.,

$$\frac{E\Phi}{RT_m^2} = An(1-x)_m^{n-1}\exp\left(-\frac{E}{RT_m}\right) \quad (5)$$

Assuming first-order kinetics ($n = 1$) and differentiating Eq. 5, neglecting small quantities, then

$$\frac{d(\ln(\Phi/T_m^2))}{d(1/T_m)} = -\frac{E}{R} \quad (6)$$

which is denoted as method (I). Therefore, one can calculate the activation energy by plotting $\ln(\Phi/T_m^2)$ versus $1/T_m$, leading to a straight line whose slope gives $-E/R$.

From the point of view of DSC kinetic analysis, the reacted fraction for a phase transition can be written in the following form:

$$x = \frac{H}{H_T} \quad (7)$$

where H_T is the total heat of transition, i.e., total area of the heat flow in heating or cooling process, H the heat of transition at t. Differentiating (7) gives

$$\frac{dx}{dt} = \frac{1}{H_T} \cdot \frac{dH}{dt} \quad (8)$$

If Eq. 8 is combined with (3), assuming $n = 1$, the following result can be obtained,

$$\frac{dx}{dT} = \frac{A}{\Phi}(1-x)\exp\left(-\frac{E}{RT}\right) \quad (9)$$

Assuming a constant heating rate Φ, the integration of (9) gives

$$-\ln(1-x) = \frac{A}{\Phi}\int_0^T \exp\left(-\frac{E}{RT}\right)dT \quad (10)$$

Let $y = E/RT$ for simplification and substitute it into (10), then

$$\frac{A}{\Phi}\int_0^T \exp\left(-\frac{E}{RT}\right)dT = \frac{AE}{\Phi R}\int_y^\infty \frac{e^{-y}}{y^2}dy$$

$$= \frac{AE}{\Phi R}\left(\frac{e^{-y}}{y} - \int_y^x \frac{e^{-y}}{y}dy\right)$$

$$= \frac{AE}{\Phi R} \cdot P(y) \quad (11)$$

where

$$P(y) = \frac{e^{-y}}{y^2}\left(1 - \frac{2!}{y} + \frac{3!}{y^2} - \frac{4!}{y^3} + \cdots\right) \quad (12)$$

Substituting Eq. 11 into 10 and taking natural logarithm on both sides, then

$$-\ln(1 - x) = \frac{AE}{\Phi R} \cdot P(y) \tag{13}$$

$$\log \Phi = \log\left[-\frac{AE}{R \cdot \ln(1-x)}\right] - 2.315 - 0.4567\frac{E}{RT} \tag{14}$$

Differentiating Eq. 14 and neglecting small quantities gives

$$\frac{\mathrm{d}(\log \Phi)}{\mathrm{d}(1/T_\mathrm{m})} = -0.4567\frac{E}{R} \tag{15}$$

which is denoted as method (II). Thus, plotting $\log \Phi$ versus $1/T_\mathrm{m}$ gives a slope equal to $-0.4567E/R$ from which the activation energy can be also obtained.

In Table 1, different parameters with reference to peak temperature T_m and heating rate Φ are summarized. Besides, the slopes calculated from two methods as mentioned above are shown in Fig. 4, respectively. The estimated activation energies are $E_1 \approx 126.3$ kJ/mol in Eq. 6 and $E_2 \approx 129.2$ kJ/mol in Eq. 15. What is the possible reason for the difference between these two results? The main basis of method (I), i.e., KAS method, is that the peak temperature of DTA signal is the temperature at which the reaction rate is a maximum. However, this assumption has been confirmed to be incorrect. The maximum reaction rate, in fact, lies somewhere before this point. On the contrary, this assumption is applicable for the DSC signal. Therefore, we can calculate activation energy of phase transition at T_p by DSC data using method (II).

Phase transition of RbH₂PO₄/SiO₂ composites at T_p

Temperature dependencies of conductivity for pure RbH₂PO₄ and $(1 - x)$RbH₂PO₄–xSiO₂ ($x = 0.3$ and 0.6) composites are presented in Fig. 5. Clearly, an abrupt increase in conductivity occurred in pure RbH₂PO₄ at T_p (~ 109 °C) with increasing temperature, which is due to structural transition from tetragonal to monoclinic phase. The same conductivity change was also observed on the cooling cycle. Therefore, the structural phase transition at T_p is reversible which agrees very well with the previous thermal analysis results. Addition of fine SiO₂ particles in RbH₂PO₄ leads to the general increase in conductivity in the investigated temperature range. In addition, the sudden

Table 1 Experimental data of DSC measurement

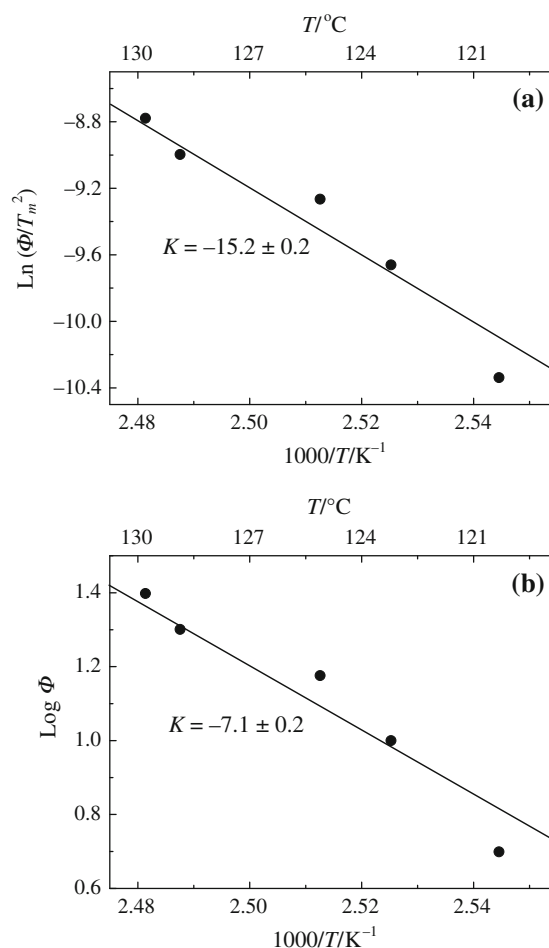| N	Φ/°C/min	T_m/°C	T_m/K	$1000/T_\mathrm{m}$/1/K	Ln (Φ/T_m^2)	Log Φ
A	5	120	393	2.54453	−10.33818	0.69897
B	10	123	396	2.52525	−9.66024	1
C	15	125	398	2.51256	−9.26485	1.17609
D	20	129	402	2.48756	−8.99717	1.30103
E	25	130	403	2.48139	−8.77890	1.39794

Fig. 4 The plots and fit lines by **a** method (I) and **b** method (II)

Fig. 5 Arrhenius plots of conductivity for $(1 - x)$RbH₂PO₄–xSiO₂ ($x = 0$, 0.3, and 0.6) with heating and cooling cycles in the temperature range from 25 to 180 °C

conductivity change at T_p disappeared, which may be attributable to the appearance of a new interface phase. We will discuss this problem in detail in later section. On the

other hand, it was found that the conductivity enhancement strongly depends on the amount of SiO_2. With increasing SiO_2 concentration, the conductivity tends to increase at both "tetragonal" and "monoclinic" phases accordingly. Therefore, the heterogeneous doping in solid acids like RbH_2PO_4 is indeed an effective method to increase its proton conductivity.

To further make clear the influence of dopant SiO_2 on the phase transition and thermal properties of RbH_2PO_4, the DSC measurements of RbH_2PO_4/SiO_2 composites were conducted in a heating–cooling cycle. Figure 6a shows the DSC curves at a fixed heating rate of 10 °C/min as a function of SiO_2 M fraction. Each heat flow was normalized by the weight of RbH_2PO_4, i.e., heat flow per 1 mg of RbH_2PO_4 in RbH_2PO_4/SiO_2 composites. One can find the endothermic peaks associated with the structural phase transition at T_p shifted slightly to higher temperature with increasing the molar ratio of SiO_2 additives. In addition, their heats of transition, which have been normalized with that in neat RbH_2PO_4, also changed with SiO_2 M ratio. In the cooling process, the addition of SiO_2 also strongly influences the phase transition of RbH_2PO_4 bulk in composites, although the exothermic peaks have no obvious shift at ~120 °C. As Fig. 6b shows, the exothermic heat flows can be separated approximately into two regions A and B. The intensity of peak A at ~120 °C reduced gradually with increasing the amount of SiO_2. Instead, the other broad peak B, appearing in the temperature range of ~95 and ~110 °C, becomes stronger and more evident. In the case of peak A and B, they should correspond to two different states of RbH_2PO_4 in the composites and be denoted as state A and state B, respectively. Furthermore, it can be noted that the total heat of transition of the exothermic peaks including A and B decrease gradually with the increase in SiO_2 content.

In order to qualitatively elucidate the relationship between heat of transition and SiO_2 M fraction in both heating and cooling process, their curves were plotted in Fig. 7. Within experimental error, the heat of transition decrease linearly with increasing SiO_2 M fraction. Besides, the heats of transition in heating and cooling process are approximately equal to each other, which indicate that the observed transformation is reversible. As for state A and B appearing in the cooling process, their molar fractions estimated roughly from their respective heat of transition were also plotted against SiO_2 M ratio in Fig. 8. With an increase in SiO_2 M ratio, the molar fraction of state A decreases linearly and disappears finally, whereas that of state B increases linearly. What is the possible reason for the gradual disappearance of state A and gradual appearance of state B with increasing SiO_2 content? According to the suggestion from Uvarov et al. [21, 22], the strong interface interaction of two components in the composite
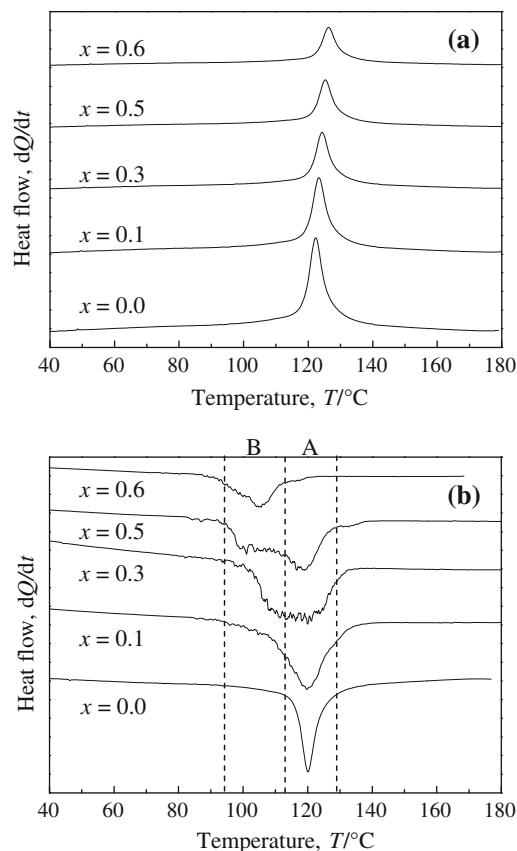

Fig. 6 DSC curves for RbH_2PO_4/SiO_2 composites with a variety of SiO_2 M fraction on **a** heating and **b** cooling cycles, at a fixed rate of 10 °C/min
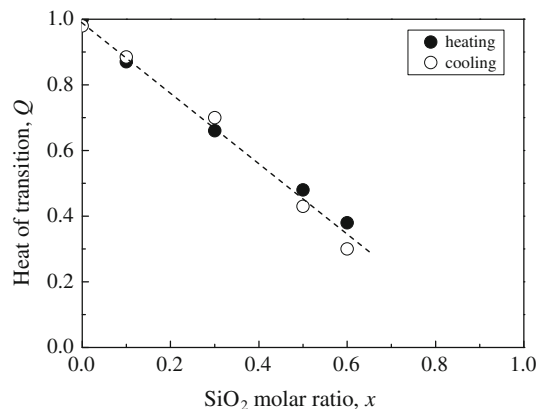

Fig. 7 Normalized heat of transition plotted against molar ratio of SiO_2 additives

leads to the formation of an interface layer on the surface of SiO_2 particles, especially in the preparation process by using a high-energy ball mill and the heating treatment. The structure of interface layer may be either epitaxial crystalline or amorphous. The amorphous phase, being disordered structurally, is the main reason for the proton conductivity
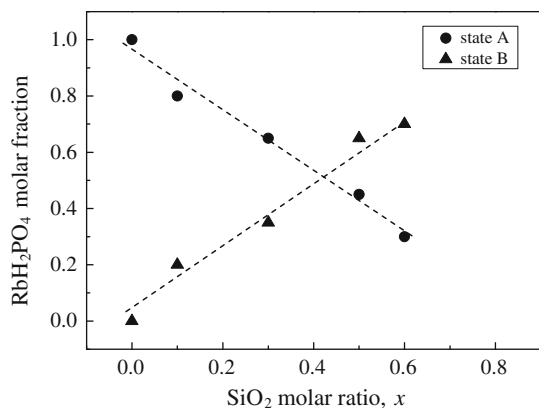
Fig. 8 Molar fraction of state A and B of RbH$_2$PO$_4$ in its composites as a function of molar ratio of SiO$_2$ additives

enhancement in RbH$_2$PO$_4$/SiO$_2$ composites, which has been confirmed in our previous report [17]. Besides, heating process further increases the adhesion energy of stabilization of interface phase on the surface of dopant particles. In other words, RbH$_2$PO$_4$ exhibited two different structures in its composites, i.e., amorphous phase and ordered bulk structure. The existence of amorphous phase facilitates ionic conductivity of composites no matter whether the phase transition from tetragonal to monoclinic at T_p takes place, which is why the jump in conductivity disappeared in RbH$_2$PO$_4$/SiO$_2$ composites. On the other hand, with increasing the content of SiO$_2$, more amorphous phase of RbH$_2$PO$_4$ formed on the surface of SiO$_2$ particles, in contrast, less tetragonal or monoclinic phase exists, leading to the attenuation of phase transition signal. This accounts for the gradual decrease in heat of transition at T_p in both heating and cooling process. Currently, further investigation of the structure and properties of interface phase is still in progress. According to the study of pure RbH$_2$PO$_4$ and comparison with its composites, heterogeneous doping by the dispersion of inert oxide particles in ionic salts influences not only its electrical properties but also thermal ones.

Conclusions

The thermal properties of RbH$_2$PO$_4$ and its composites, especially at T_p, have been studied with the help of DSC measurements. The conclusions are summarized below:

(1) RbH$_2$PO$_4$ undergoes a structural transition from tetragonal to monoclinic phase at $T_p \approx 109$ °C, resolving the dispute in literatures as to its origin. Besides, the endothermic peak temperature (T_m) presents a linear relationship with square root of heating rate ($\Phi^{1/2}$).

(2) Two calculation methods were used to estimate the activation energy of phase transition at T_p, i.e., $E_1 \approx 126.3$ kJ/mol and $E_2 \approx 129.2$ kJ/mol, respectively. The difference between them is attributed to their different assumption and prerequisite.

(3) The conductivity of RbH$_2$PO$_4$/SiO$_2$ composites strongly depends on the SiO$_2$ content. With increasing the molar fraction of SiO$_2$, the conductivity enhancement takes place and the sudden conductivity change disappears at T_p.

(4) In RbH$_2$PO$_4$/SiO$_2$ composites, heat of transition at T_p decreases gradually with an increase in SiO$_2$ amount. A fresh exothermic peak B between ~ 95 and ~ 110 °C appeared in cooling process, which may be attributable to the existence of amorphous phase of RbH$_2$PO$_4$.

References

1. Haile SM, Boysen DA, Chisholm CRI, Merle RB. Solid acids as fuel cell electrolytes. Nature. 2001;410:910–3.
2. Boysen DA, Uda T, Chisholm CRI, Haile SM. High-performance solid acid fuel cells through humidity stabilization. Science. 2004;303:68–70.
3. Metcalfe B, Clark JB. Differential scanning calorimetry of RbH$_2$PO$_4$ and CsH$_2$PO$_4$. Thermochim Acta. 1978;24:149–53.
4. Blinc R, O'Reilly DE, Peterson EM, Williams JM. High-temperature phase transition in RbH$_2$PO$_4$. J Chem Phys. 1969;50:5408–11.
5. Blinc R, Ferraro JR, Postmus C. Effects of high pressure on the far-infrared spectra of paraelectric KH$_2$PO$_4$ and RbH$_2$PO$_4$. J Chem Phys. 1969;51:732–7.
6. Averbuch-Pouchot MT, Durif A. Structure of a new form of rubidium dihydrogen phosphate, RbH$_2$PO$_4$. Acta Crystallogr C. 1985;41:665–7.
7. Baranov AI, Khiznichenko VP, Shuvalov LA. High-temperature phase transition and proton conductivity in some KDP-family crystals. Ferroelectrics. 1989;100:135–41.
8. Boysen DA, Haile SM. Conductivity of potassium and rubidium dihydrogen phosphates at high temperature and pressure. Chem Mater. 2004;16:693–7.
9. Lee KS. Hidden nature of the high-temperature phase transition in crystals of KH$_2$PO$_4$-type: is it a phase change? J Phys Chem Solids. 1996;57:333–42.
10. Ortiz E, Vargas RA, Cuervo G, Mellander BE, Gustafson J. On the high-temperature phase transition of RbH$_2$PO$_4$—a polymorphic transition? J Phys Chem Solids. 1998;59:1111–7.
11. Ortiz E, Vargas RA, Mellander BE. On the high-temperature phase transitions of some KDP-family compounds: a structural phase transition? A transition to a bulk-high proton conducting phase? Solid State Ion. 1999;125:177–85.
12. Park JH, Lee KS, Choi BC. High-temperature transformation in KH$_2$PO$_4$ and RbH$_2$PO$_4$ crystals. J Phys Condens Matter. 2001;13:9411–9.
13. Park JH. Possible origin of the proton conduction mechanism of CsH$_2$PO$_4$ crystals at high temperatures. Phys Rev B. 2004;69:0541041–6.

14. Ponomareva VG, Uvarov NF, Lavrova GV, Hairetdinov EF. Composite protonic solid electrolytes in the $CsHSO_4$-SiO_2 system. Solid State Ion. 1996;90:161–6.

15. Ponomareva VG, Lavrova GV. Influence of dispersed TiO_2 on protonic conductivity of $CsHSO_4$. Solid State Ion. 1998;106: 137–41.

16. Ponomareva VG, Lavrova GV, Simonova LG. The influence of heterogeneous dopant porous structure on the properties of protonic solid electrolyte in the $CsHSO_4$–SiO_2 system. Solid State Ion. 1999;118:317–23.

17. Li ZK. Impedance analysis and protonic conduction mechanism in RbH_2PO_4/SiO_2 composite systems. Electrochim Acta. Accepted for publication.

18. Li ZK, Tang TB. High-temperature thermal behaviors of XH_2PO_4 (X = Cs, Rb, K, Na) and LiH_2PO_3. Thermochim Acta. 2010;501: 59–64.

19. Boysen DA, Haile SM. High-temperature behavior of CsH_2PO_4 under both ambient and high pressure conditions. Chem Mater. 2003;15:727–36.

20. Sanchez-Jimenez PE, Criado JM, Perez-Maqueda LA. Kissinger kinetic analysis of data obtained under different heating schedules. J Therm Anal Calorim. 2008;94:427–32.

21. Uvarov NF, Vanek P. Stabilization of new phases in ion-conducting nanocomposites. J Mater Synth Process. 2000;8:319–26.

22. Uvarov NF, Bokhonov BB, Politov AA, Vanek P, Petzelt J. Interface-stabilized states of silver iodide in AgI–Al_2O_3 composites. J Mater Synth Process. 2000;8:327–32.